Article

Large-Scale Oceanic Variability Associated with the Madden-Julian Oscillation during the CINDY/DYNAMO Field Campaign from Satellite Observations

Toshiaki Shinoda [1,*]**, Tommy G. Jensen** [1]**, Maria Flatau** [2]**, Sue Chen** [2]**, Weiqing Han** [3] **and Chunzai Wang** [4]

[1] Naval Research Laboratory, Stennis Space Center, MS 39529, USA;
E-Mail: tommy.jensen@nrlssc.navy.mil

[2] Naval Research Laboratory, Monterey, CA 93943, USA;
E-Mails: maria.flatau@nrlmry.navy.mil (M.F.); sue.chen@nrlmry.navy.mil (S.C.)

[3] Department of Atmospheric and Oceanic Sciences, University of Colorado, Boulder, CO 80309, USA; E-Mail: weiqing.han@colorado.edu

[4] NOAA AOML, Miami, FL 33149, USA; E-Mail: chunzai.wang@noaa.gov

* Author to whom correspondence should be addressed; E-Mail: toshiaki.shinoda@nrlssc.navy.mil; Tel.: +1-228-688-5356.

Abstract: During the CINDY/DYNAMO field campaign (fall/winter 2011), intensive measurements of the upper ocean, including an array of several surface moorings and ship observations for the area around 75°E–80°E, Equator-10°S, were conducted. In this study, large-scale upper ocean variations surrounding the intensive array during the field campaign are described based on the analysis of satellite-derived data. Surface currents, sea surface height (SSH), sea surface salinity (SSS), surface winds and sea surface temperature (SST) during the CINDY/DYNAMO field campaign derived from satellite observations are analyzed. During the intensive observation period, three active episodes of large-scale convection associated with the Madden-Julian Oscillation (MJO) propagated eastward across the tropical Indian Ocean. Surface westerly winds near the equator were particularly strong during the events in late November and late December, exceeding 10 m/s. These westerlies generated strong eastward jets (>1 m/s) on the equator. Significant remote ocean responses to the equatorial westerlies were observed in both Northern and Southern Hemispheres in the central and eastern Indian Oceans. The anomalous SSH associated with strong eastward jets propagated eastward as an equatorial Kelvin wave and generated

intense downwelling near the eastern boundary. The anomalous positive SSH then partly propagated westward around 4°S as a reflected equatorial Rossby wave, and it significantly influenced the upper ocean structure in the Seychelles-Chagos thermocline ridge about two months after the last MJO event during the field campaign. For the first time, it is demonstrated that subseasonal SSS variations in the central Indian Ocean can be monitored by Aquarius measurements based on the comparison with *in situ* observations at three locations. Subseasonal SSS variability in the central Indian Ocean observed by RAMA buoys is explained by large-scale water exchanges between the Arabian Sea and Bay of Bengal through the zonal current variation near the equator.

1. Introduction

While the Madden-Julian Oscillation (MJO; [1]) has been intensively studied in the past few decades by observations, numerical modeling, and theories [2], most state-of-the-art coupled climate models are unable to simulate its salient features such as the coherent eastward propagation and the magnitude of intraseasonal convection [3,4]. Also, prediction skills of the MJO in current global forecast systems are very low, particularly during its initiation over the Indian Ocean. Accordingly, a thorough understanding of key processes involved in the MJO initiation in the Indian Ocean is crucial for the improvement of climate model simulations and prediction. The Cooperative Indian Ocean experiment on intraseasonal variability (CINDY)/Dynamics of the MJO (DYNAMO) international field program was thus designed to collect *in situ* observations over the Indian Ocean to advance our understanding of the MJO initiation processes and to improve MJO prediction [5]. One of the primary targets of the field campaign is the role of air-sea interaction in MJO initiation, and thus oceanic processes are of the great importance because they are fundamental in determining sea surface temperature (SST).

CINDY/DYNAMO field observations were conducted during late 2011 and early 2012, and include an array of enhanced surface moorings and ship observations for the area around 75°E–80°E, Equator-10°S in the central Indian Ocean [5]. Upper ocean observations include Conductivity Temperature Depth (CTD) profiler, shipboard Acoustic Doppler Current Profilers (ADCPs), thermistor chains, and microstructure profilers from research vessels. Several surface and subsurface moorings were also deployed to monitor upper ocean current, temperature, salinity and turbulence. Furthermore, vertical profiles of temperature and salinity were collected by numerous Airborne Expendable Bathythermograph (AXBTs) and Airborne Expendable Conductivity Temperature Depth (AXCTDs) from aircrafts.

During the field campaigns, three active episodes of large-scale convection and anomalous surface zonal winds associated with the MJO propagated eastward across the tropical Indian Ocean (Figure 1). Accordingly, upper-ocean variability associated with these MJO events were well monitored in the CINDY/DYNAMO observational areas. While the analysis of these high resolution data in the central Indian Ocean will help understand potentially crucial processes of MJO initiation, aspects of the

large-scale variations also need to be described, which complements the analysis of the data collected during the field campaign. In addition, these MJO events are unique in that two strong episodes of atmospheric convection occurred within one month (late November-December) without a clear suppressed phase between the events (Figure 1), and thus it is likely that a strong ocean response to surface forcing fields associated with these unusual events is observed in broad areas in the tropical Indian Ocean during this period.

Because of the recent development of satellite observations, large-scale variability of the surface and upper ocean can be described on the subseasonal time scale especially in the tropics based on the analysis of satellite-derived data. For example, the time and space resolutions of recent satellite altimetry products are substantially improved, and it is now feasible to detect the signals of 10–17 day period SSH variability associated with oceanic equatorial waves, e.g., [6–8]. Also, the recent launch of Aquarius/SAC-D satellite enables us to describe subseasonal variability of surface salinity produced by tropical instability waves [9]. Furthermore, near-surface ocean velocity derived from satellite measurements [10] is shown to be reliable for studies on many aspects of tropical ocean variability, e.g., [11–13].

Figure 1. (**Left**): A longitude-time diagram of Outgoing Longwave Radiation (OLR) [14] averaged over 10°N–10°S. The dashed line (at 80°E) indicates the location of CINDY/DYNAMO ocean observations. (**Right**): Same as the left panel except for the surface zonal wind anomaly derived from the NCEP/NCAR reanalysis [15]. The anomaly is calculated by subtracting the annual cycle for the period 1979–2011.
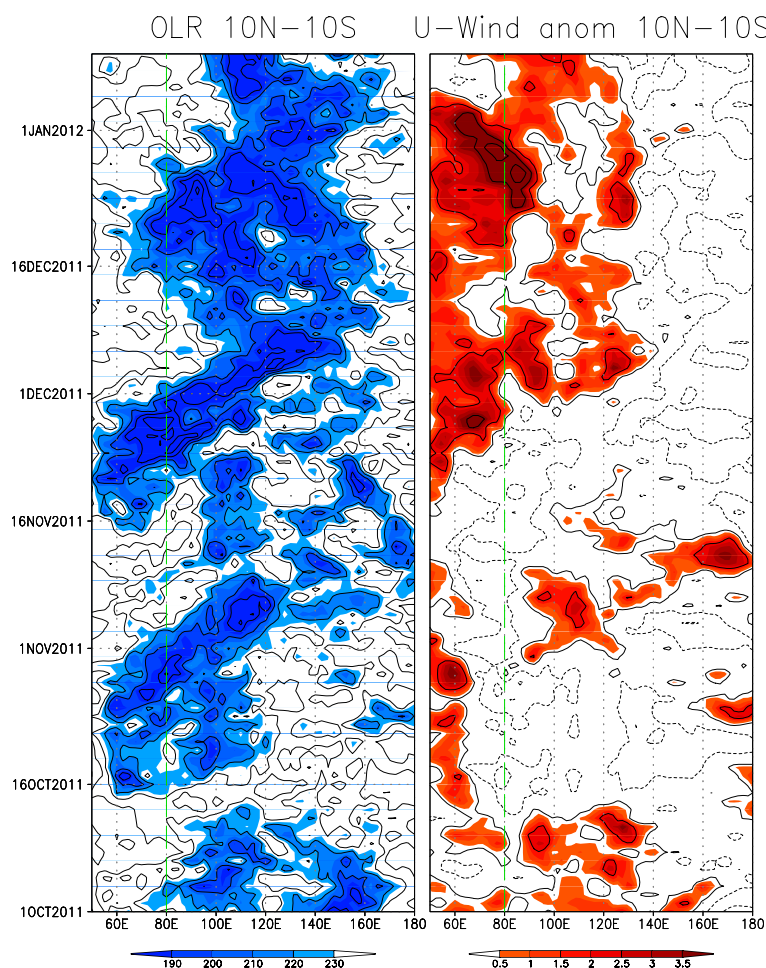
In this paper, large-scale variations of the upper ocean surrounding the CINDY/DYNAMO arrays and locations of ship observations are described based on the satellite-derived data to provide a context for the future analysis of the data collected during the field campaign. In particular, the large-scale variation of the equatorial jet, changes in spatial pattern of surface salinity due to the equatorial jet, and the remote oceanic response to the MJO-induced surface forcing fields through reflected Rossby waves are emphasized.

2. Data

We use six primary data sets derived from satellite observations in this study. These satellite derived data are compared with *in situ* measurements in the tropical Indian Ocean.

Near-surface velocity data, derived from the Ocean Surface Current Analysis–Real time (OSCAR) project [11], are used to describe the spatial pattern of surface currents during the CINDY/DYNAMO field campaign. The OSCAR velocities are estimated using sea surface height (SSH) data from satellite altimeter measurements, surface wind stress, and drifter data, and they are presented in the form of 5-day average near-surface velocity fields on a 1° × 1° grid. Subseasonal variations in SSH are identified using daily multi-satellite analyses of SSH anomalies. These analyses are obtained from Archiving, Validation, and Interpretation of Satellite Oceanographic (AVISO) data.

Weekly sea surface salinity (SSS) data on the 1° × 1° grid derived from Aquarius measurements [16,17] are used to describe subseasonal salinity variability associated with MJO events in the entire tropical Indian Ocean. Aquarius is a focused program to provide the global SSS variability needed for climate studies, which is a collaborative effort between NASA and the Argentinian Space Agency Comisión Nacional de Actividades Espaciales (CONAE). SSS is measured by the Aquarius instrument aboard the Aquarius/Satélite de Aplicaciones Científicas (SAC)-D aircraft. There are about 3% of missing data for the analysis period in the tropical Indian Ocean, which are interpolated in space using inverse distance weighting. The Aquarius and OSCAR data are linearly interpolated to daily resolution for compatibility with other daily data.

Precipitation from TRMM 3B42 product [18] is used to describe rainfall variability associated with MJO events. We use the 3-hourly average precipitation on a 0.25° × 0.25° grid. Surface winds from Windsat measurements [19] are used to describe subseasonal surface wind variability. We use 3-day average 10-m height winds on 0.25° × 0.25° grid. Winds are estimated from WindSat microwave brightness temperatures measurements. Daily SST data on 0.25° × 0.25° grid from the blended product of satellite/*in situ* observations [20] are also used to describe SST variability associated with the MJO events during CINDY/DYNAMO.

In situ data from the Research Moored Array for African-Asian-Australian Monsoon Analysis and Prediction (RAMA) program [21] are used to evaluate satellite-derived data. We use the daily mean salinity, temperature, current and SST data from the buoy measurements. These comparisons include near surface salinity data at three locations along 80.5°E (1.5°S, 4°S and 8°S) during fall 2011 when large subseasonal SSS variations associated with MJO events were observed.

3. Results

3.1. Westerly Wind Events Associated with the MJO

During the MJO events in late November and late December 2011, strong anomalous surface westerly winds near the equator were observed (Figure 1). In order to validate the Windsat data in the tropical Indian Ocean including the strong westerlies, the data are compared with *in situ* observations. Figure 2 shows the zonal winds at 10 m height from Windsat, the RAMA buoy and the NCEP/NCAR reanalysis [15] at the two buoy locations on the equator during fall/winter 2011. Zonal winds at 4 m measured by the RAMA buoy are extrapolated to 10 m using air temperature, humidity at 2 m and SST with the TOGA COARE bulk flux algorithm version 3.0 [22]. Windsat data can capture the strong westerly wind events in late November and late December (Figure 2), in good agreement with RAMA buoy observations. Note that the NCEP/NCAR reanalysis fails to capture or underestimate westerly wind events, in particular at 90°E.

To describe the spatial pattern of these equatorial westerly wind events and their connection to winds in off-equatorial areas, average surface winds during the events are calculated. During the late November event (23–30 November), equatorial westerly winds extend in the almost entire Indian Ocean, and they are associated with cyclonic circulation in the Arabian Sea (Figure 3(a)). The strongest equatorial westerlies, which exceed 10 m/s, are found north of the equator around 0°N–3°N, 76°E–79°E.

Figure 2. (**Upper**): 3-day average zonal winds (m/s) at 10 m height at 80.5°E, equator from Windsat (red), RAMA buoy (green), and the NCEP/NCAR reanalysis (black). (**Lower**): Same as upper panel except at 90°E, equator.
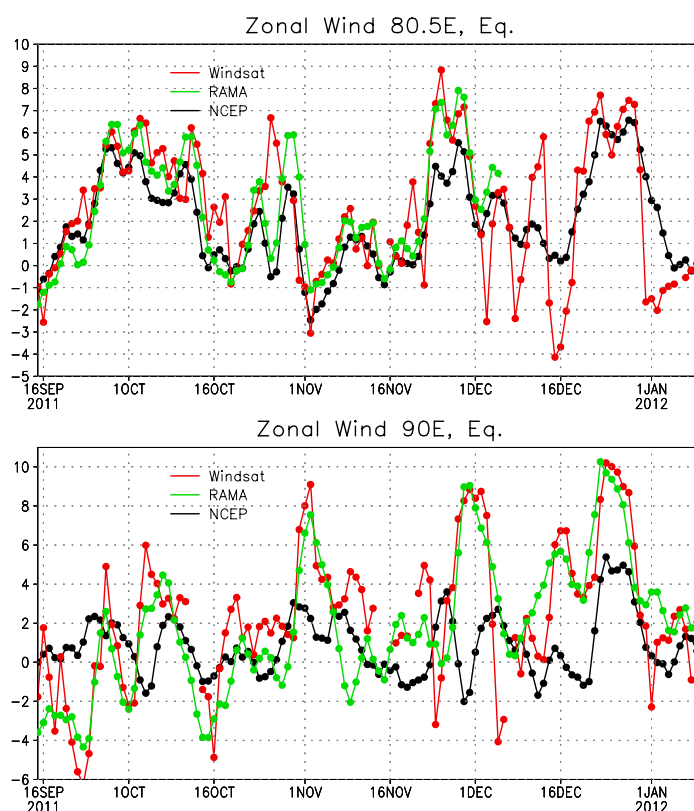
Surface winds during the late December event (22–31 December) are displayed in Figure 3(b). Strong equatorial winds are confined to the central and eastern Indian Ocean east of 70°E during this event. These equatorial westerlies are connected to a strong cyclonic circulation in the Bay of Bengal, which is centered around 10°N, 90°E. The strongest equatorial zonal winds are found south of the equator around 6°S–1°S, 75°E–90°E. The maximum zonal winds on the equator exceed 10 m/s (Figure 2).

Figure 3. (**a**) Average winds (m/s) at 10 m (arrows) and wind speed (shading) from Windsat during 23–30 November 2011. (**b**) Same as (**a**) except the periods 22–31 December 2011.
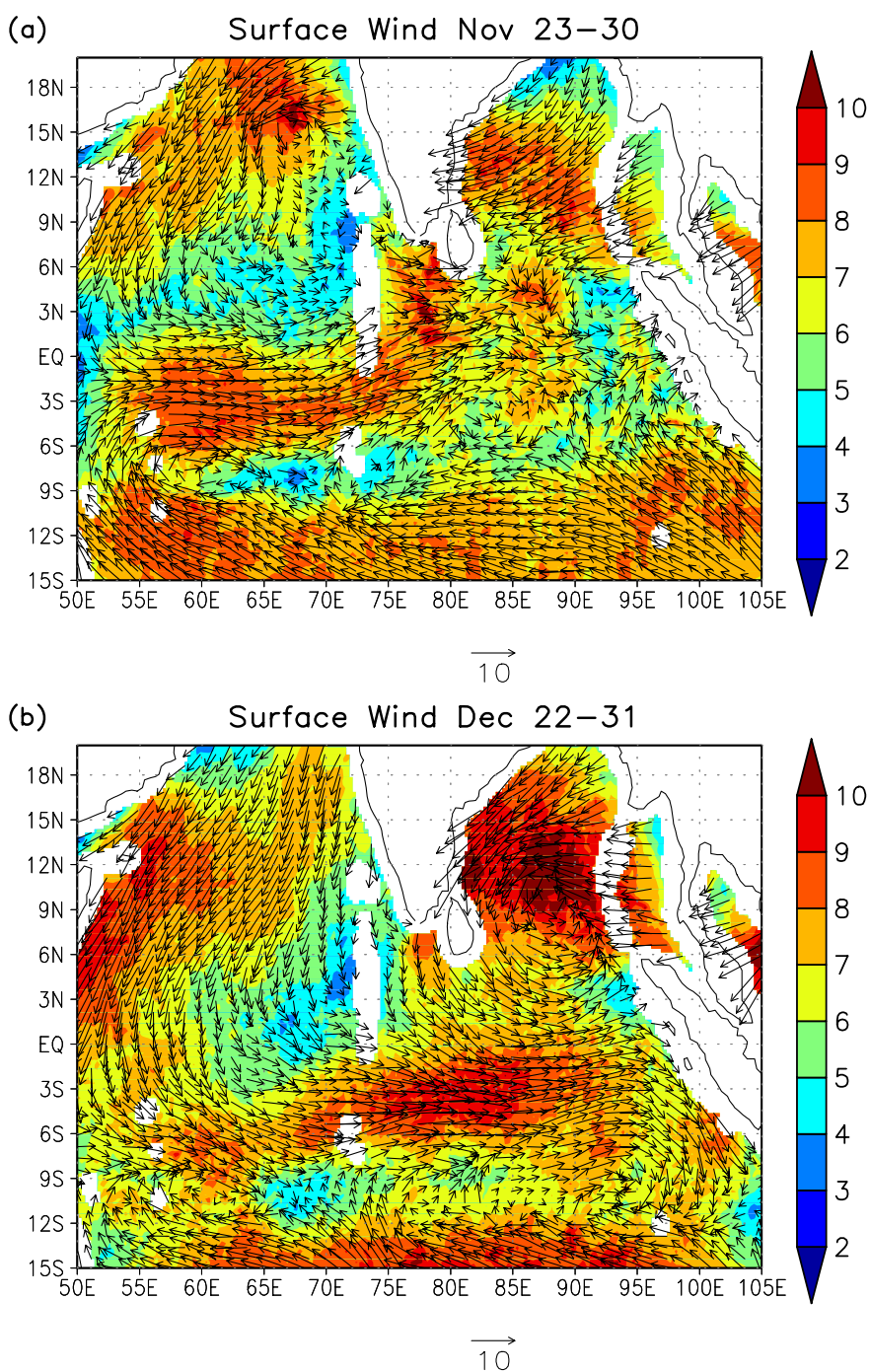
3.2. Local Ocean Response to Westerly Wind Events

3.2.1. Dynamical Response: Equatorial Jet and SSH

In the equatorial oceans, a strong zonal jet centered on the equator can be accelerated in response to zonal wind variations [23]. Accordingly, strong westerly wind events associated with the MJO often generate strong oceanic equatorial jets in the central and eastern Indian Oceans, e.g., [24]. In order to validate the equatorial zonal current from OSCAR data, the zonal velocity component at 80.5°E and 90°E on the equator are compared with the RAMA buoy data. A strong eastward jet in late November and early December is found in the OSCAR data at 80.5°E and 90°E, but the jet at 80.5°E in late December is underestimated (Figure 4). The equatorial jet in late December is stronger at 90°E than at 80.5°E in the OSCAR analysis.

Figure 4. Zonal current (m/s) at 10 m at 80.5°E, equator (blue line) and 90°E, equator (red line) from OSCAR, and at 80.5°E, equator from the RAMA buoy (green line).
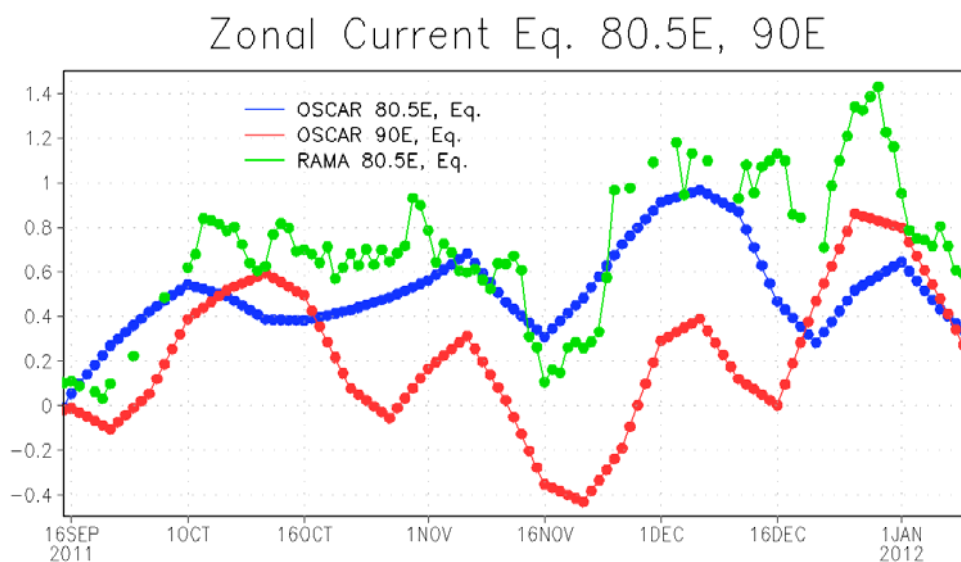

Figure 5 displays the longitude-time diagram of zonal velocity from the OSCAR analysis. A large zonal extent of the equatorial jet in late November–December is found. While the maximum zonal velocity in early December is located around 80°E (near the RAMA buoy site), a strong jet is generated in the eastern part of the basin in late December. Since the RAMA buoy (80.5°E, Equator) is located near the edge of strong zonal current in late December, it is not surprising that the agreement between the OSCAR and RAMA zonal current at this location is rather poor at that time (Figure 4).

Westerly winds associated with the MJO also generate equatorial Kelvin waves, which can be detected from SSH time series, e.g., [25–29]. In association with strong anomalous zonal currents in late November–December, SSH near the equator also varies substantially (Figure 5). The positive SSH anomalies propagate eastward during late November to mid-December, and the phase speed is consistent with that of first baroclinic mode equatorial Kelvin wave. Note that the eastward propagation is not clearly evident in the zonal velocity. This could be partly because both Kelvin and Rossby waves contribute to equatorial zonal velocity, e.g., [30].

SSH near the eastern boundary starts increasing from early December, and continues to increase until mid-January. The maximum SSH anomaly, which exceeds 10 cm, occurs in early to mid-January after the strongest jet is generated. In late December, large positive SSH anomalies are found in a large area (10°N–10°S) near the eastern boundary (Figure 6). In particular, large anomalies, which exceed 10 cm, are found near the coast of Sumatra around 2°S–6°S.

Figure 5. (**Left**): Longitude-time diagram of near surface zonal velocity (m/s) averaged over 1°N–1°S from OSCAR. (**Right**) Same as left panel except for sea surface height (SSH) anomaly (cm) derived from altimeter measurements. The white line indicates the phase speed of 2.8 m/s.
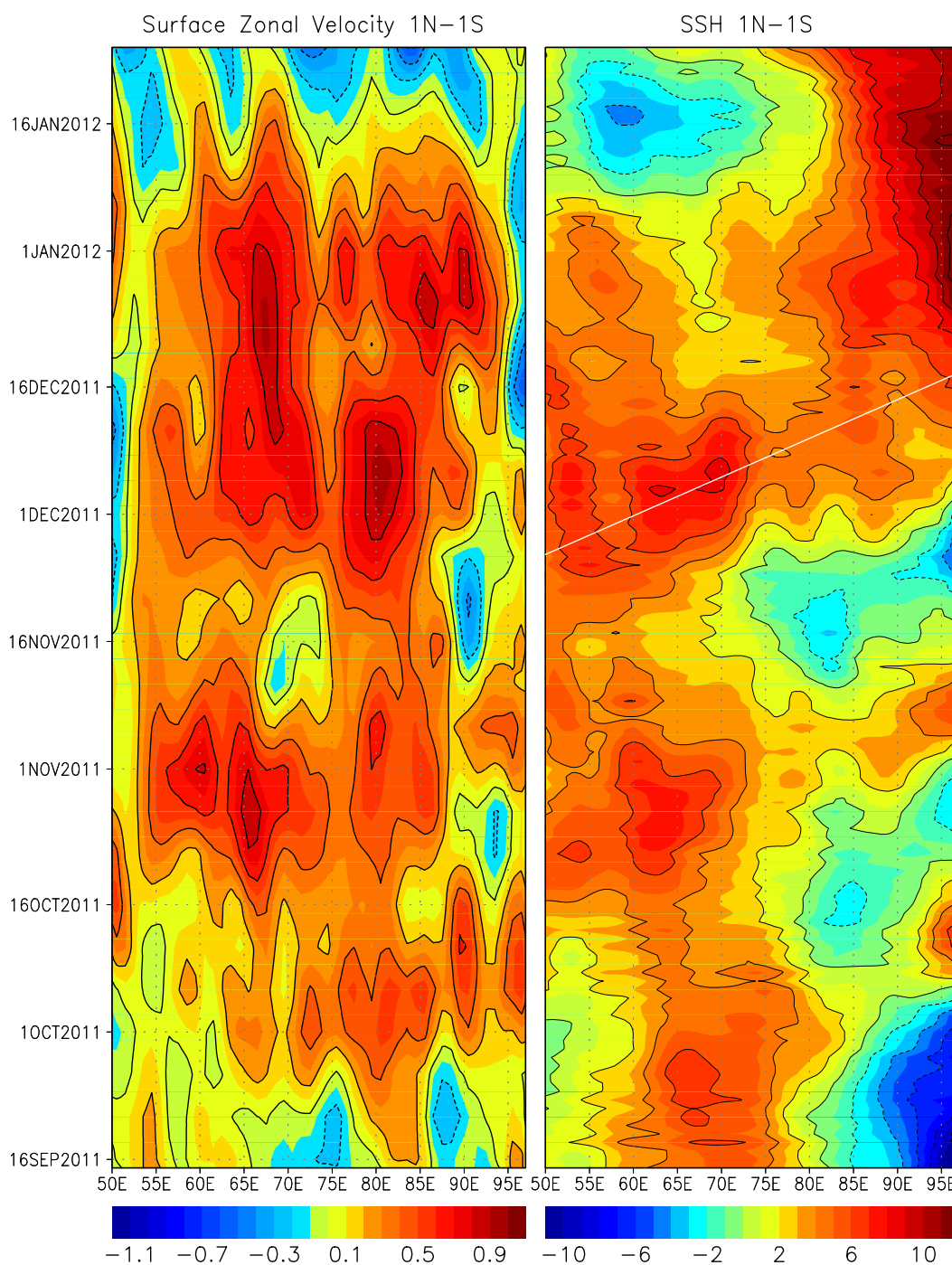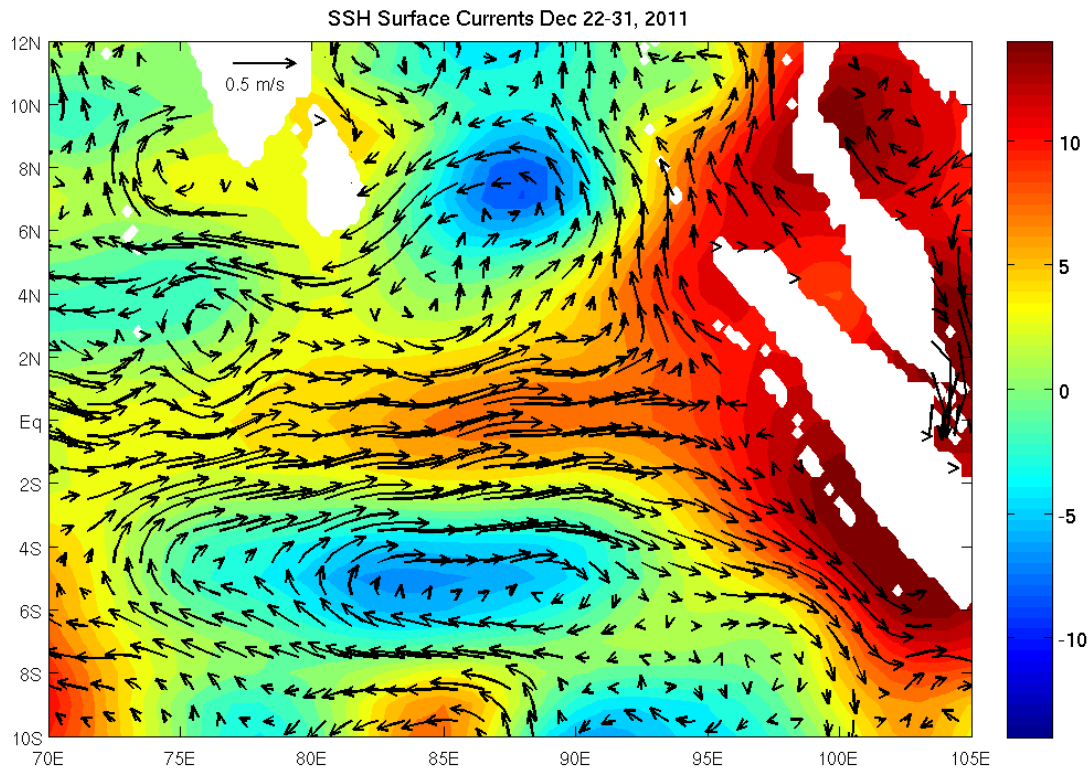
Figure 6. Average SSH anomaly (cm; shading) from altimetry and surface currents (m/s; arrows) from OSCAR during 22–31 December 2011.

SSH Surface Currents Dec 22-31, 2011

3.2.2. Sea Surface Temperature

Significant SST variations in the tropical Indian and western Pacific warm pool regions are generally observed during the MJO events because of anomalous surface fluxes of heat and momentum, e.g., [31–36]. Figure 7 shows the SST at 80.5°E, equator from high resolution blended analysis and RAMA buoy data. A substantial cooling (~1.5 °C) occurs from late November to early January, which is well captured by the blended SST analysis. The spatial pattern of the cooling is described by calculating the SST difference between the periods of 15–22 November 2011 and 28 December 2011–3 January 2012 (Figure 8). A significant cooling, which exceeds 1 °C, is found in the almost entire tropical Indian Ocean north of 10°S during this period. Since this cooling is the impact of two consecutive MJO events in late November and December without a clear suppressed phase between the two, the magnitude of cooling is larger than other typical MJO events, e.g., [24,33]. Near the eastern boundary between 5°N and 10°S, a significant warming is found, in contrast to other areas near the equator. A similar warming is found in other MJO events [24]. This could be due to the deepening of the thermocline along the coast of Sumatra during this period (Figure 6). However, analyses of subsurface temperature and currents from observations and numerical models are necessary to examine further details of the processes that control the SST variation in this area.

Figure 7. Time series of sea surface temperature (SST) from the RAMA buoy (green line) and from the SST analysis [20] (blue line).
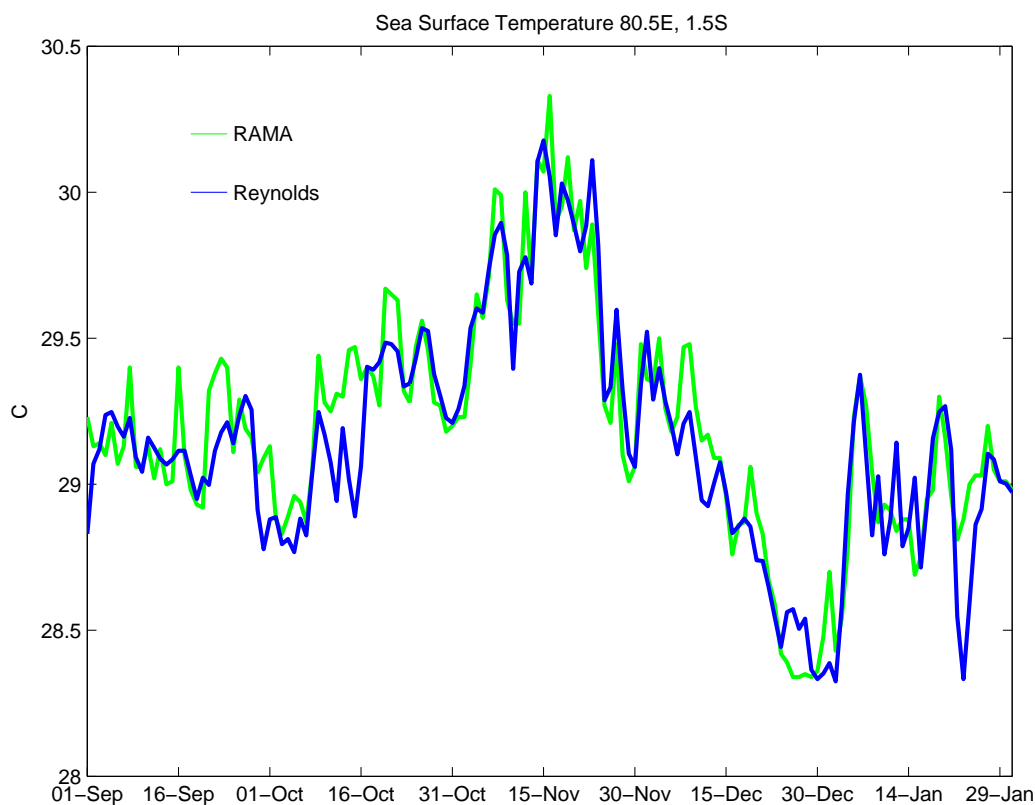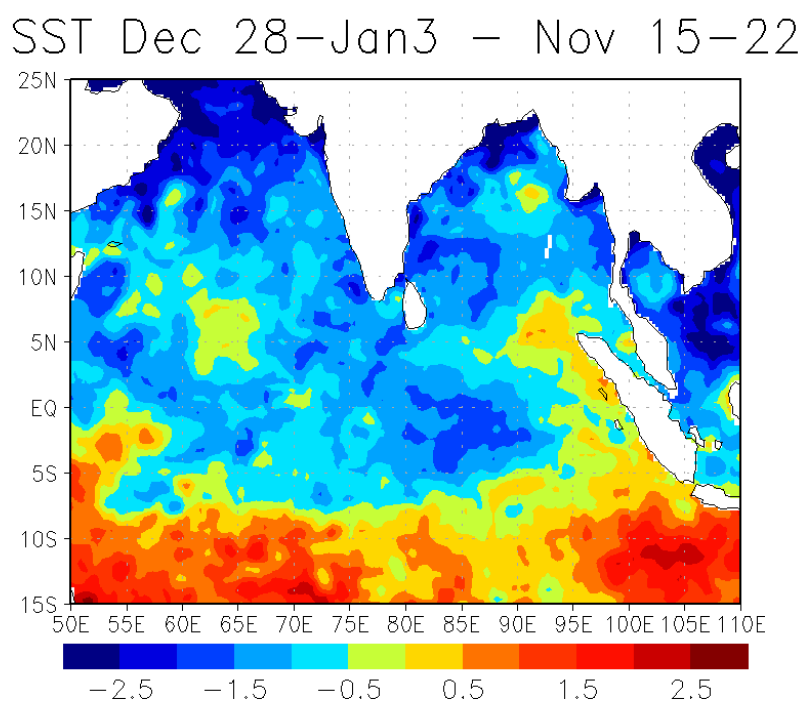

Figure 8. Average SST (°C) during 28 December 2011–3 January 2012 minus that during 15–22 November 2011 based on the SST analysis [20].

3.3. Remote Response to the MJO Events

In the previous section, it is demonstrated that large positive SSH anomalies are found along the eastern boundary in late December-early January right after the strong equatorial jet is generated. These SSH anomalies could propagate westward by radiating Rossby waves from the eastern boundary, e.g., [37–41].

Figure 9 shows the longitude-time diagram of SSH at 4°N and 4°S. Signals of westward propagation are found in both the Northern and Southern Hemispheres from late December. In the Southern Hemisphere, two distinct signals of the propagation, which are consistent with the phase speed of first and second baroclinic mode Rossby waves, are evident during January–early March, 2012. Because of these Rossby waves, there are significant positive SSH anomalies (and thus deep thermocline) in the large area (55°E–95°E) of the equatorial Indian Ocean in late February. A prominent deepening of the thermocline at 80.5°E, 4°S during late January–early February, when downwelling Rossby waves pass at this location, is clearly evident in the temperature profiles observed by the RAMA buoy (Figure 10). The 20 °C isotherm depth, which is in the middle of main thermocline, changes about 40–50 m during this period. After the deepening of the thermocline, SST increases about 1 °C at this location by late February.

Figure 9. Longitude-time diagram of SSH anomaly (cm) at 4°S (**left**) and 4°N (**right**). The white lines indicate the phase speed of −0.66 m/s and −0.33 m/s.
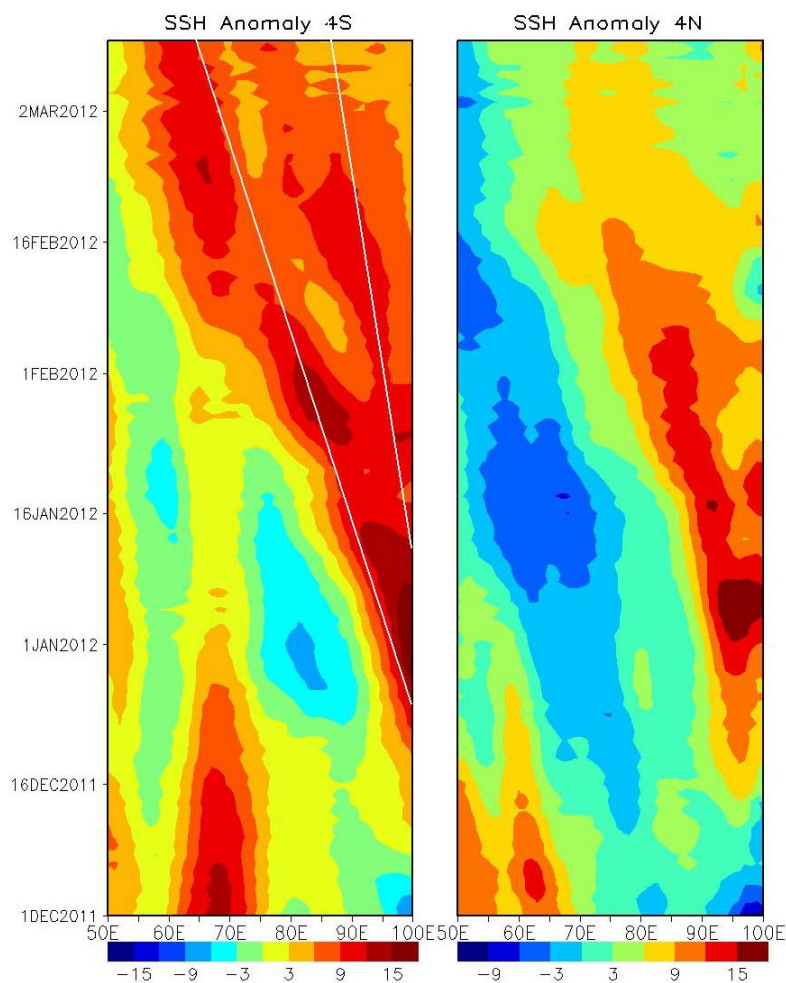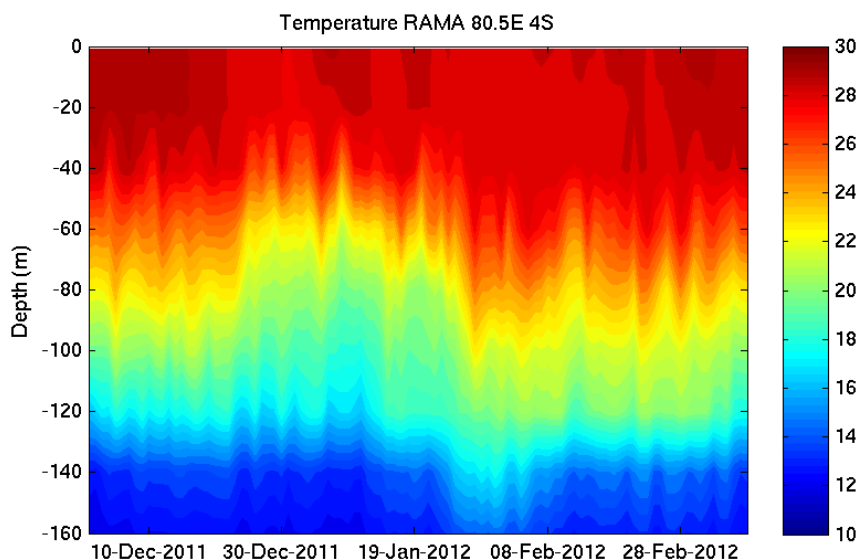
Figure 10. Time series of temperature (°C) profile from the RAMA buoy at 4°S, 80.5°E.

The latitude (4°S) shown in Figures 9 and 10 corresponds to a northern part of the Seychelles–Chagos thermocline ridge (SCTR), which is a zonal region of upwelling (around 2.5°S–14°S) generated by Ekman divergence [42,43]. Because of the shallow thermocline in the SCTR, the SST is more sensitive to the changes in thermocline depth than surrounding areas, e.g., [44,45]. Hence significant variability of the thermocline depth in February–early March caused by Rossby wave propagation may impact SST in this region. Although signals of SST anomalies along the path of reflected Rossby waves during this period are not clearly evident (not shown), changes in heat content due to these waves may influence the upper ocean response to local surface forcing in the SCTR.

Recent studies [41,46] suggest that reflected Rossby waves, originally generated from Kelvin waves forced by westerly winds associated with the MJO, may cause the significant SST change in the central Indian Ocean, and this anomalous SST could further act as a trigger of the initiation of convection for generating a subsequent MJO event. During March 2012, atmospheric convection was initiated in the central Indian Ocean, and it was developed to a MJO event that propagated to the western Pacific in late March [5]. Coupled modeling studies are necessary to examine whether these reflected Rossby waves actually influenced the MJO initiation during March 2012.

In the Northern Hemisphere, Rossby waves are damped around 75°E. This could be partly due to the influence of land around Sri Lanka and South India. Nevertheless, SSH signals are significant, and thus they could influence the SST in the Bay of Bengal.

3.4. Surface Salinity

Because of the large contrast of upper ocean salinity between the Bay of Bengal and the Arabian Sea, near-surface salinity in the central Indian Ocean in the vicinity of the equator varies substantially through the variation of zonal currents [47–49]. Since strong equatorial currents on the subseasonal timescale are often generated in the central Indian Ocean, e.g., [24,50–51], the upper ocean salinity could fluctuate largely on the subseasonal time scale.

Because of the recent development and advancement of microwave radiometer and the analysis technique, sea surface salinity is shown to be monitored from satellite observations [16,17,52]. A

recent study [9] indicates that SSS fluctuations associated with tropical instability waves can be detected by the Aquarius measurements in the eastern tropical Pacific where a large meridional gradient of climatological SSS is located. Since a large subseasonal fluctuation of SSS is found in the central Indian Ocean due to a large zonal gradient of climatological SSS, the Aquarius data may detect subseasonal SSS variability in this region. In order to examine the feasibility of monitoring subseasonal SSS variation by the Aquarius measurements in the tropical Indian Ocean, the Aquarius SSS is first compared with *in situ* salinity observed by surface moorings in the central Indian Ocean during the CINDY/DYNAMO period. Then large-scale SSS along with the satellite-derived near surface currents in the tropical Indian Ocean is described, explaining subseasonal SSS variations observed by surface moorings in the central Indian Ocean.

SSS from Aquarius during September to December 2011 is compared with near-surface salinity measured by RAMA moorings. Figure 11 shows SSS at 1.5°S, 4°S, and 8°S along 80.5°E from Aquarius and the salinity at 1 m depth measured by RAMA buoys. SSS variations during this period from Aquarius agree reasonably well with those measured by RAMA moorings at these locations. No obvious systematic bias is found in the Aquarius SSS at 1.5°S and 4°S, 80.5°E. The Aquarius SSS at 8°S, 80.5°E is lower than RAMA measurements by about 0.2 psu during most of the period. Near the equator at 1.5°S, 80.5°E, SSS increases from late October to mid-November. Then SSS starts decreasing in late November, and continues to decrease in December. At 8°S, 80.5°E, SSS decreases during the entire period. In contrast, SSS is nearly constant at 4°S, 80.5°E.

To gain further insights into this latitudinal difference in SSS variations observed by the RAMA array, the large-scale SSS and surface current pattern during early to mid-November are described (Figure 12). During this period, the zonal current direction is eastward in the central Indian Ocean between 3°N and 3°S around 80.5°E. Although anomalous zonal winds are weak in the central Indian Ocean during this period (Figure 1), eastward currents are generally observed on the equator during this season because of the monsoon transition [53]. These eastward currents bring high salinity waters from the Arabian Sea, and thus SSS in this region tends to increase. Westward currents are found north of 4°N and south of 5°S around 80.5°E. Since the southern branch of westward currents extends to the vicinity of the eastern boundary, fresher waters originating from the Bay of Bengal are advected to the central Indian Ocean, and they affect the SSS near the southern RAMA buoy site (8°S, 80.5°E). The northern branch of the westward currents is associated with the southward currents along the coast of Sri Lanka, which carry low salinity waters directly from the Bay of Bengal. Around 3°S–5°S, the zonal currents are very weak and the zonal salinity gradient is small.

The large-scale pattern of SSS and surface currents described above are consistent with the salinity observed at RAMA buoy sites at 1.5°S, 4°S and 8°S along 80.5°E. Although OSCAR velocity and Aquarius salinity are independent estimates based on different satellite observations, spatial variations of these two variables are consistent. In the central Indian Ocean around 80.5°E, the latitudes where eastward currents are found (3°N–3°S) correspond to the areas of relatively high salinity while the regions where westward currents are evident (north of 4°N and south of 5°S) are the areas of relatively low salinity. This suggests that the latitudinal difference of salinity variations observed at RAMA buoy sites along 80.5°E is caused by exchanges of the Arabian Sea saltier waters and the Bay of Bengal fresher waters.

Figure 11. Time series of sea surface salinity (psu) in boreal fall 2011 estimated from Aquarius (blue line) and RAMA buoy (green line) at 80.5°E, 1.5°S (**top**), 80.5°E, 4°S (**middle**), and 80.5°E, 8°S (**bottom**).
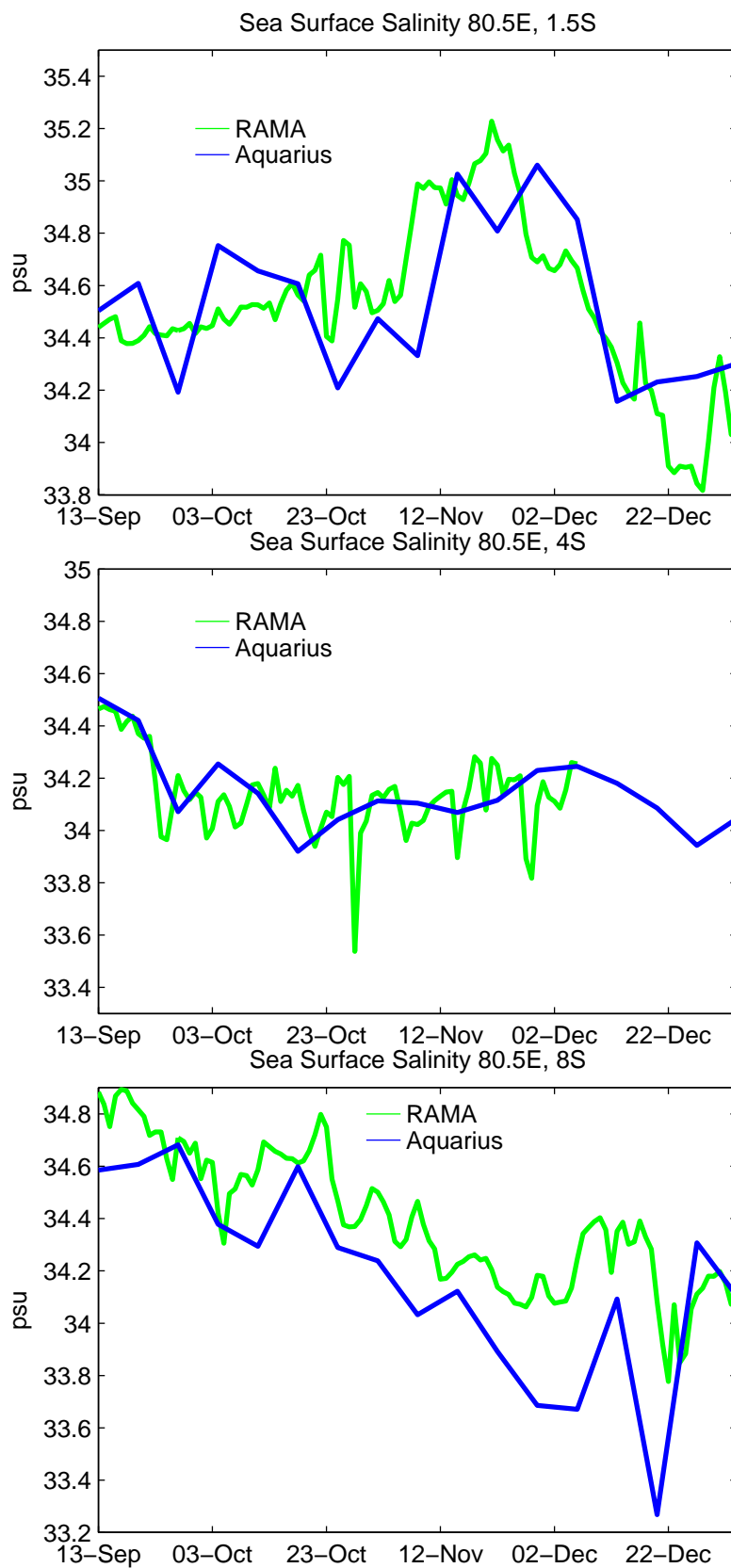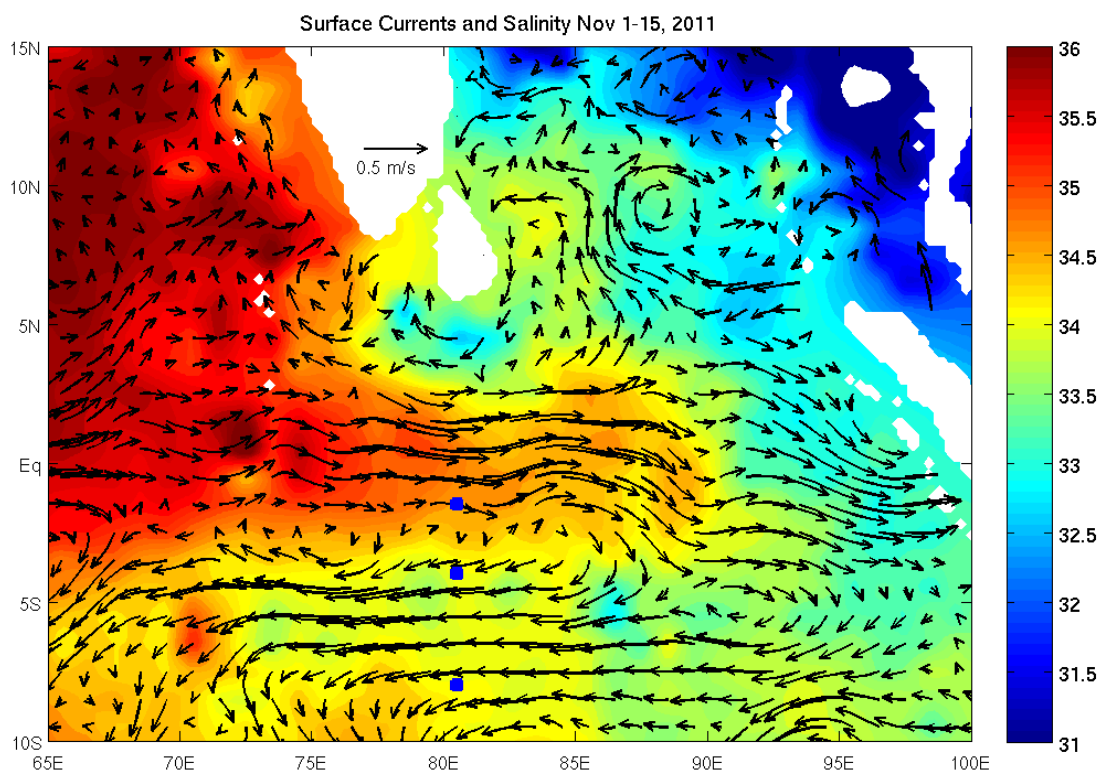
Figure 12. Average SSS (psu) derived from Aquarius measurements and near surface currents (m/s) from OSCAR during 1–15 November. RAMA buoy locations along 80.5°E are indicated by blue closed square marks. SSS data are interpolated to 0.2° × 0.2° grid.


In late November 2011, a large-scale episode of atmospheric convection associated with the MJO has been generated in the central Indian Ocean as discussed in the previous section. Heavy precipitation is observed from November 23 near the equator (Figure 13(a)). A significant amount of precipitation associated with the MJO convection in late November is found in the large area of the central Indian Ocean (Figure 13(c)), especially near the equator between 3°N and 3°S. These large-scale surface freshwater fluxes may cause the decrease of salinity in the central tropical Indian Ocean including the RAMA buoy site near the equator (1.5°S, 80.5°E; Figure 11).

The strong westerly wind event, which exceeded 9 m/s, was observed on the equator in the central Indian Ocean on November 24, and it generated a strong eastward equatorial jet exceeding 1 m/s (Figure 13(b)). The acceleration of the jet is also found in the OSCAR current data, as discussed in Section 3.2. The strong eastward currents tend to cause the salinity to be higher in the central Indian Ocean by advecting high salinity Arabian Sea waters. However, the surface salinity decreases during late November-early December, suggesting that the impact of surface freshwater fluxes is larger than horizontal advection and the entrainment of saltier waters below the mixed layer for generating surface salinity variations.

During the CINDY/DYNAMO field campaign, vertical profiles of salinity, temperature, and microstructure in the upper ocean as well as surface freshwater fluxes were monitored in the equatorial central Indian Ocean. These high resolution data will help quantify the impact of the entrainment (vertical mixing) of high salinity waters on the surface salinity variation. Also, numerical model experiments validated by these data could quantify the relative importance of surface flux, horizontal advection and vertical mixing for upper ocean salinity variability in this region.

Figure 13. (**a**) Time series of precipitation averaged over 75°E–90°E, 3°N–3°S. (**b**) Time series of zonal wind and current at Equator, 80.5°E. Green lines indicate zonal current at 10 m depth from the RAMA buoy, and blue lines indicate near surface zonal current from OSCAR. Red dashed lines indicate zonal winds at 4m height measured by the RAMA buoy. (**c**) Average precipitation from TRMM 3B42 during 23–30 November 2011.
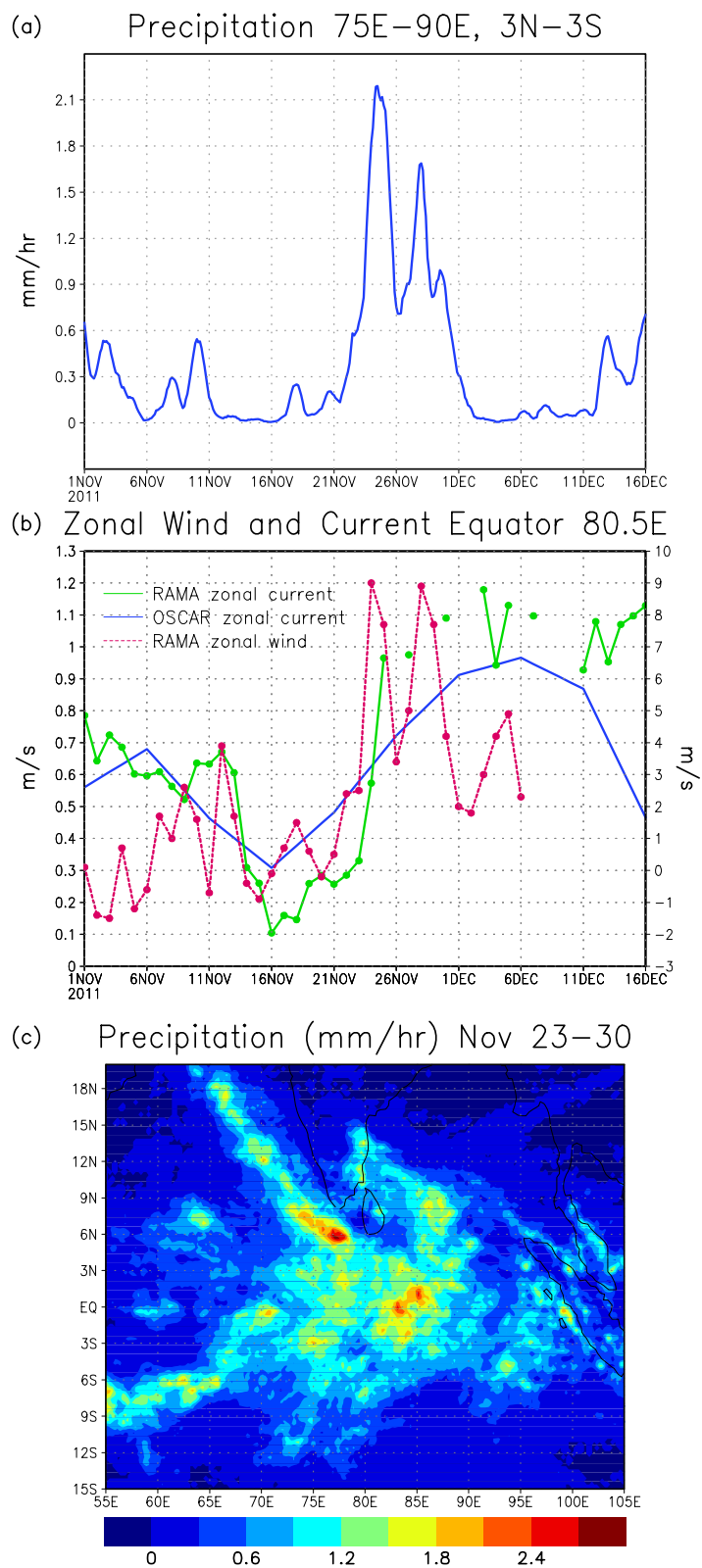
4. Summary and Discussion

The CINDY/DYNAMO international field program was designed to collect *in situ* observations for the purpose of advancing the understanding of MJO initiation processes and ultimately improving MJO prediction. During boreal fall and winter 2011, the intensive field observations were conducted, which include an array of enhanced surface moorings and observations on research vessels for the area around 75°E–80°E, Equator-10°S in the central Indian Ocean. In this study, large-scale variations of the upper ocean surrounding the CINDY/DYNAMO arrays and locations of ship observations are described based on the satellite-derived data to provide a context for future analysis of the data collected during the field campaign.

Surface currents, sea surface height (SSH), sea surface salinity (SSS), surface winds and sea surface temperature (SST) during the CINDY/DYNAMO field campaign derived from satellite observations are analyzed. During the field campaign, three active episodes of large-scale convection and anomalous surface zonal winds associated with the MJO propagated eastward across the tropical Indian Ocean. Surface westerly winds near the equator were particularly strong during the MJO events in late November and late December, exceeding 10 m/s. These wind events generated strong eastward jets, which exceed 1 m/s, on the equator in the central and eastern Indian Ocean. In late December–early January, a large increase of positive SSH anomalies (and thus deep thermocline) was found in the large area (10°N–10°S) near the eastern boundary in association with strong equatorial jets. These SSH anomalies then partly propagated westward around 4°S and 4°N as reflected Rossby waves. The Rossby waves around 4°S caused significant positive SSH anomalies in the region of the Seychelles–Chagos thermocline ridge about two months after the last MJO event observed during the field campaign. The magnitude of large-scale SST cooling during the MJO events in late November and December is larger than that in other typical MJO events since these events are unique in that two strong episodes of atmospheric convection occurred within one month without a clear suppressed phase between the events.

We demonstrate that large-scale subseasonal surface salinity variation associated with the MJO in the Indian Ocean can be detected by the recent satellite measurements (Aquarius) based on the comparison with *in situ* observations and with satellite-derived near surface velocity fields. The comparison of SSS from Aquarius with the RAMA buoy observations shows a reasonably good agreement for the subseasonal variation. The large-scale patterns of SSS and near-surface current are consistent with each other, and also consistent with the salinity variation measured by RAMA moorings. In the central Indian Ocean near the equator, high salinity waters from the Arabian Sea were advected in early November, 2011, and the increase of SSS in this region was observed by the RAMA buoy during this period. South of the equator between 5°S and 9°S, westward currents brought fresher waters originating from the Bay of Bengal, causing a decrease of SSS at 8°S, 80.5°E, which was also observed by the RAMA buoy.

Because of the recent advancement of a variety of satellite observations, large-scale ocean variability on the subseasonal time-scale in the tropical Indian Ocean can now be described, as demonstrated in this study. However, satellite data cannot provide the vertical structure of currents, temperature and salinity, which are important for understanding physical processes associated with subseasonal ocean variability. In particular, monitoring vertical profiles of upper ocean variables are

crucial for identifying processes that control SST such as ocean mixing caused by strong current shear. During the CINDY/DYNAMO field campaign, substantial amount of high resolution data in the upper ocean, including the microstructure, have been collected in the central Indian Ocean, and the data are expected to be available in the near future. A combination of high quality data from *in situ* measurements (CINDY/DYNAMO), large-scale description of surface variables from satellite data (this study), and numerical modeling validated by these data will hopefully help identify key processes for the MJO initiation.

In this study, it is also demonstrated for the first time that large-scale subseasonal SSS variability in the tropical Indian Ocean can be monitored by the Aquarius data reasonably well. Therefore, the data would be useful for many purposes including the computation of large-scale freshwater budget and numerical model validations. Also, the assimilation of the data into ocean models would provide products that could be used to investigate the importance of upper ocean salinity stratification for a variety of phenomena in the tropical Indian Ocean.

Acknowledgments

References

1. Madden, R.A.; Julian, P.R. Description of global-scale circulation cells in the tropics with a 40–50 day period. *J. Atmos. Sci.* **1972**, *29*, 1109–1123.
2. Zhang, C. Madden-Julian oscillation. *Rev. Geophys.* **2005**, *43*, RG2003.
3. Lin, J.-L.; Kiladis, G.N.; Mapes, B.E.; Weickmann, K.M.; Sperber, K.R.; Lin, W.; Wheeler, M.C.; Schubert, S.D.; Del Genio, A.; Donner, L.J.; *et al.* Tropical intraseasonal variability in 14 IPCC AR4 climate models. Part I: Convective signals. *J. Clim.* **2006**, *19*, 2665–2690.
4. Hung, M.-P.; Lin, J.-L.; Wang, W.; Kim, D.; Shinoda, T.; Weaver, S.J. MJO and convectively coupled equatorial waves simulated by CMIP5 climate models. *J. Clim.* **2013**, in press.
5. Yoneyama, K.; Zhang, C.; Long, C.N. Tracking pulses of the Madden-Julian oscillation. *Bull. Amer. Meteorol. Soc.* **2013**, in press.
6. Shinoda, T. Observed dispersion relation of Yanai Waves and 17-day tropical instability waves in the Pacific Ocean. *SOLA* **2010**, *6*, 17–20.
7. Shinoda, T. Observation of first and second baroclinic mode Yanai waves in the ocean. *Quart. J. Roy. Meteor. Soc.* **2012**, *138*, 1018–1024.
8. Farrar, J.T.; Durland, T.S. Wavenumber-frequency spectra of inertia-gravity and mixed rossby-gravity waves in the equatorial Pacific Ocean. *J. Phys. Oceanogr.* **2012**, *42*, 1859–1881.

9. Lee, T.; Lagerloef, G.; Gierach, M.M.; Kao, H.-Y.; Yueh, S.; Dohan, K. Aquarius reveals salinity structure of tropical instability waves. *Geophys. Res. Lett.* **2012**, *39*, L12610.

10. Lagerloef, G.S.E.; Mitchum, G.T.; Lukas , R.B.; Niiler, P.P. Tropical Pacific near-surface currents estimated from altimeter, wind, and drifter data. *J. Geophys. Res.* **1999**, *104*, 313–326.

11. Bonjean, F.; Lagerloef, G.S.E. Diagnostic model and analysis of the surface currents in the tropical Pacific Ocean. *J. Phys. Oceanogr.* **2002**, *32*, 2938–2954.

12. Shinoda, T.; Kiladis, G.N.; Roundy, P.E. 2009: Statistical representation of equatorial waves and tropical instability waves in the Pacific Ocean. *Atmos. Res.* **2009**, *94*, 37–44.

13. Shinoda, T.; Hurlburt, H.E.; Metzger, E.J. Anomalous tropical ocean circulation associated with La Nina Modoki. *J. Geophys. Res. Oceans* **2011**, *116*, C12001.

14. Liebmann, B.; Smith, C.A. Description of a complete (interpolated) outgoing longwave radiation dataset. *Bull. Amer. Meteorol. Soc*. **1996**, *77*, 1275–1277.

15. Kalnay, E.; Kanamitsu, M.; Kistler, R.; Collins, W.; Deaven, D.; Gandin, L.; Iredell, M.; Saha, S.; White, G.; Woollen, J.; *et al.* The NCEP/NCAR 40-year reanalysis project. *Bull. Amer. Meteorol. Soc.* **1996**, *77*, 437–471.

16. Lagerloef, G.; Colomb, F.R.; Le Vine, D.; Wentz, F.; Yueh, S.; Ruf, C.; Lilly, J.; Gunn, J.; Yi, C.; Decharon, A.; *et al.* The Aquarius/SAC-D mission: Designed to meet the salinity remote-sensing challenge. *Oceanography* **2008**, *21*, 68–81.

17. Lagerloef, G.; Wentz, F.; Yueh, S.; Kao, H.-Y.; Johnson, G.C.; Lyman, J.M. Aquarius satellite mission provides new, detailed view of sea surface salinity—State of the climate in 2011. *Bull. Amer. Meteorol. Soc*. **2012**, *93*, S70–S71.

18. Huffman, G.J.; Adler, R.F.; Bolvin, D.T.; Gu, G.; Nelkin, E.J.; Bowman, K.P.; Stocker, E.F.; Wolff, D.B. The TRMM multi-satellite precipitation analysis: Quasi-global, multi-year, combined-sensor precipitation estimates at fine scale. *J. Hydrometeor*. **2007**, *8*, 33–55.

19. Gaiser, P.W.; Germain, K.M.S.; Twarog, E.M.; Poe, G.A.; Purdy, W.; Richardson, D.; Grossman, W.; Jones, W.L.; Spencer, D.; Golba, G.; *et al.* The WindSat space borne polarimetric microwave radiometer: Sensor description and early orbit performance. *IEEE Trans. Geosci. Remote Sens.* **2004**, *42*, 2347–2361.

20. Reynolds, R.W.; Smith, T.M.; Liu, C.; Chelton, D.B.; Casey, K.S.; Schlax, M.G. Daily high-resolution-blended analyses for sea surface temperature. *J. Clim.* **2007**, *20*, 5473–5496.

21. McPhaden, M.J.; Meyers, G.; Ando, K.; Masumoto, Y.; Murty, V.S.N.; Ravichandran, M.; Syamsudin, F.; Vialard, J.; Yu, L.; Yu, W. RAMA: The research moored array for African-Asian-Australian monsoon analysis and prediction. *Bull. Amer. Meteorol. Soc.* **2009**, *90*, 459–635.

22. Fairall, C.; Bradley, E.F.; Rogers, D.P.; Edson, J.B.; Young, G.S. The TOGA COARE bulk flux algorithm. *J. Geophys. Res.* **1996**, *101*, 3747–3764.

23. Yoshida, K. A theory of the cromwell current and of the equatorial upwelling-an interpretation in a similarity to a coastal circulation. *J. Oceanogr. Soc. Jpn*. **1959**, *15*, 159–170.

24. Shinoda, T.; Jensen, T.; Flatau, M.; Chen, S. Surface wind and upper ocean variability associated with the Madden-Julian Oscillation simulated by the Coupled Ocean/Atmosphere Mesoscale Prediction System (COAMPS). *Mon. Wea. Rev*. **2013**, in press.

25. Kessler, W.S.; McPhaden, M.J.; Weickmann, K.M. Forcing of intraseasonal Kelvin waves in the equatorial Pacific Ocean. *J. Geophys. Res*. **1995**, *100*, 10613–10631.

26. Cravatte, S.; Picaut, J.; Eldin, G. Second and first baroclinic Kelvin modes in the equatorial Pacific at intraseasonal time scales. *J. Geophys. Res*. **2003**, *108*, 3266.

27. Roundy, P.E.; Kiladis, G.N. Observed relationships between oceanic Kelvin waves and atmospheric forcing. *J. Clim.* **2006**, *19*, 5253–5272.

28. Shinoda, T.; Roundy, P.E.; Kiladis, G.N. Variability of intraseasonal Kelvin waves in the equatorial Pacific Ocean. *J. Phys. Oceanogr*. **2008**, *38*, 921–944.

29. Iskandar, I.; McPhaden, M.J. Dynamics of wind-forced intraseasonal zonal current variations in the equatorial Indian Ocean. *J. Geophys. Res*. **2011**, *116*, C06019.

30. Nagura, M.; McPhaden, M.J. The dynamics of wind-driven intraseasonal variability in the equatorial Indian Ocean. *J. Geophys. Res*. **2012**, *117*, C02001.

31. Krishnamurti, T.N.; Osterhof, D.K.; Mehta, A.V. Air-Sea interaction on the time scale of 30 to 50 days. *J. Atmos. Sci*. **1988**, *45*, 1304–1322.

32. Zhang, C. Atmospheric intraseasonal variability at the surface in the tropical western Pacific Ocean. *J. Atmos. Sci*. **1996**, *53*, 739–758.

33. Shinoda, T.; Hendon, H.H.; Glick, J. Intraseasonal variability of surface fluxes and sea surface temperature in the tropical western Pacific and Indian Ocean. *J. Clim.* **1998**, *11*, 1685–1702.

34. Shinoda, T.; Hendon, H.H. Mixed layer modeling of intraseasonal variability in the tropical western Pacific and Indian Oceans. *J. Clim.* **1998**, *11*, 2668–2685.

35. Shinoda, T.; Hendon H.H. Upper ocean heat budget in response to the Madden-Julian Oscillation in the western equatorial Pacific. *J. Clim*. **2001**, *14*, 4147–4165.

36. Woolnough, S.J.; Slingo, J.M.; Hoskins, B.J. The relationship between convection and sea surface temperature on intraseasonal timescales. *J. Clim.* **2000**, *13*, 2086–2104.

37. Jensen, T.G. Equatorial variability and resonance in a wind-driven Indian Ocean model. *J. Geophys. Res*. **1993**, *98*, 22533–22552.

38. Han, W. Origins and dynamics of the 90-day and 30-60 day variations in the equatorial Indian Ocean. *J. Phys. Oceanogr*. **2005**, *35*, 708–728.

39. Han, W.; Yuan, D.; Liu, W.T.; Halkides, D.J. Intraseasonal variability of Indian Ocean sea surface temperature during boreal winter: MJO *versus* submonthly forcing and processes. *J. Geophys. Res*. **2007**, *112*, C04001.

40. Oliver, E.C.J.; Thompson, K.R. Madden-Julian oscillation and sea level: Local and remote forcing. *J. Geophys. Res.* **2010**, *115*, C01003.

41. Webber, B.G.M.; Matthews A.J.; Heywood, K.J. A dynamical ocean feedback mechanism for the Madden–Julian oscillation. *Quart. J. Roy. Meteorol. Soc*. **2010**, *136*, 740–754.

42. McCreary, J.P.; Kundu, P.K.; Molinari, R.L. A numerical investigation of dynamics, thermodynamics and mixed-layer processes in the Indian Ocean. *Progr. Oceanogr*. **1993**, *31*, 181–244.

43. Hermes, J.C.; Reason, C.J.C. Annual cycle of the South Indian ocean (Seychelles–Chagos) thermocline ridge in a regional ocean model. *J. Geophys. Res*. **2008**, *113*, C04035.

44. Xie, S-P.; Annamalai, H.; Schott, F.A.; McCreary, J.P. Structure and mechanism of South Indian Ocean climate variability. *J. Clim*. **2002**, *15*, 864–878.

45. Duvel, J.P.; Roca, R.; Vialard, J. Ocean mixed layer temperature variations induced by intraseasonal convective perturbations over the Indian Ocean. *J. Atmos. Sci.* **2004**, *61*, 1004–1023.

46. Webber, B.G.M.; Matthews, A.J.; Heywood, K.J.; Stevens, D.P. Ocean Rossby waves as a triggering mechanism for primary Madden–Julian events. *Quart. J. Roy. Meteorol. Soc.* **2012**, *138*, 514–527.

47. Jensen, T.G. Arabian Sea and Bay of Bengal exchange of salt and tracers in an ocean model. *Geophys. Res. Lett.* **2001**, *28*, 3967–3970.

48. Schott, F.; McCreary, J.P. The monsoon circulation of the Indian Ocean. *Progr. Oceanogr.* **2001**, *51*, 1–123.

49. Grunseich, G.; Subrahmanyam, B.; Arguez, A. Influence of the Madden-Julian Oscillation on sea surface salinity in the Indian Ocean. *Geophys. Res. Lett.* **2011**, *38*, L17605.

50. Shinoda, T.; Han, W. Influence of Indian Ocean dipole on atmospheric subseasonal variability. *J. Clim.* **2005**, *18*, 3891–3909.

51. Sengupta D.; Senan, R.; Goswami, B.N.; Vialard, J. Intraseasonal variability of equatorial Indian Ocean zonal currents. *J. Clim.* **2007**, *20*, 3036–3055.

52. Font, J.; Boutin, J.; Reul, N.; Spurgeon, P.; Ballabrera-Poy, J.; Chuprin, A.; Gabarró, C.; Gourrion, J.; Guimbard, S.; Hénocq, C.; *et al.* SMOS first data analysis for sea surface salinity determination. *Int. J. Remote Sens.* **2012**, *34*, 3654–3670.

53. Wyrtki, K. An equatorial jet in the Indian Ocean. *Science* **1973**, *181*, 262–264.